IIETA International Information and Engineering Technology Association
Advancing the World of Information and Engineering

Mathematical Modelling of Engineering Problems
Vol. 11, No. 11, November, 2024, pp. 2919-2928
Journal homepage: http://iieta.org/journals/mmep

Effect of Tail Water Depth on Characteristics of Hydraulic Jump Formed Downstream of Stepped Weir

May S. Saleh[1*], Shaymaa A.M. Al-Hashimi[1], Abdul-Sahib T. Al-Madhhachi[1,2]

[1] Department of Water Resources Engineering, College of Engineering, Mustansiriyah University, Baghdad 10047, Iraq
[2] Civil and Environmental Engineering, Oklahoma State University Stillwater 74078, OK, USA

Corresponding Author Email: maysamir@uomustansiriyah.edu.iq

https://doi.org/10.18280/mmep.111105

Received: 22 July 2023
Revised: 11 December 2023
Accepted: 25 December 2023
Available online: 29 November 2024

Keywords:
open channel, hydraulic jump, numerical CFD model, Fluent, VOF, stepped weir, tail water

ABSTRACT

In our work, experimental tests were conducted to study the hydraulic jump's characteristics forming in a flume with rectangular cross section. A broad crested weir with one step is used to produce a hydraulic jump downstream the flume. A 2D ANSYS-Fluent model version 20, which is a powerful tool used to simulate hydraulic problems with complex geometry, was used. Volume of fluid (VOF) method with a (k–ε) realizable turbulent model was applied to simulate the hydraulic jump for different flow conditions. After validating the numerical model with experimental data, it was then used to calculate sequent depths and velocity contours and to predict the location of the hydraulic jump formed in the flume. Different tail water depths were produced for different flowrate values by adjusting the opening of the tail gate located at the end of the channel. The water surface profiles obtained from the numerical model were in good agreement with those obtained using the physical model, as confirmed by a statistical analysis employing some standard error indexes. Thus, the numerical model can effectively estimate the hydraulic jump location. Results showed that the distance to hydraulic jump increases as the sequent depth decreases due to increasing tail gate opening. For most flow conditions, the depth of the tail water is slightly lower than the sequent depth. The relative height of the hydraulic jump located near the downstream was low and had shorter roller lengths than that located near the weir. Therefore, it is classified as undular jump. Some relations between studied variable are presented in the following section.

1. INTRODUCTION

Occurrence of hydraulic jumps in open channels take many forms according to the nature of channel, the tested hydraulic structure, and the target study. Generally, this phenomenon can be defined as a transformation of flow state from high-velocity, super-critical flow to low-velocity, sub-critical flow.

Hydraulic jump formed downstream the broad-crested weir was widely studied given its effective dissipation for flow energy. Turbulent hydraulic jumps have been modeled using various computational analyses and laboratory investigations. Salmasi and Özger [1] conducted a series of experiments with different numbers of steps and slops of weir. The authors developed a model using a neuro-fuzzy approach, and this model was performed with experimental data. This model is found to be more accurate in estimating the relative energy dissipation than regression analysis. Al-Husseini et al. [2] utilized 10 models of cascade weirs with a pooled step, one of which had a sluice gate upstream and an ordinary weir. Their effects on improving energy dissipation were investigated. The results showed that the obtained energy dissipation was maximum when a sluice gate at the upstream of a pooled step was placed. The ratio of holes to weir area of 7.15% was the most effective in energy dissipation. Khatibi et al. [3] carried out a series of laboratory experiments to study the hydraulic properties of flow over a stepped gabion weir. The authors used multiple regression analysis based on artificial neural network (ANN) and gene expression programming (GEP). The result showed that energy dissipation computed based on ANN is more reliable than that computed by GEP. Good agreement was found between the experimental results and ANN results. Sauida and Ahsan [4] also utilized ANN model to estimate the features of hydraulic jump formed downstream the multigates. The authors conducted a series of laboratory experiments to generate data that were used to train, verify, and test the ANN model. The result showed that ANN model can calculate the energy loss downstream the multigates. Ibrahim et al. [5] used a new technique for dissipating the energy of hydraulic jump formed downstream the weir. In the new approach, five rows of bed water jets were installed on smooth apron to examine their efficiency in dissipating the jump energy. Different discharge values with different tail water depth were used. The result showed that the middle raw of jets improved the dissipation efficiency of hydraulic jump up to 70.8%, and the jump length decreases compared with the non-jetted case. Felder et al. [6] studied the effect of inflow

variation on the jump characteristics for flow under sluice gate. The author found that the free surface profile, roller length, and jump toe were highly affected by the condition of inflow. When the inflow condition is fully developed, the jump length was shorter than that under the condition of partially developed inflow. In addition, Mohammadi et al. [7] presented a novel method for estimating the length of the jump created on the correspondence of the jump and wall-jet turbulence including the gradient of pressure, considering the effect of the flow curvature and the slight increase in water surface profile at the end of the jump. The authors used the 1D momentum equation to present an expression for conjugate depths in term of Froude numbers and step height. The proposed method can be accurately used for large values of initial Froude number. Abdel-Mageed [8] investigated the effect of channel slope on the jump characteristics (such as jump length, sequent depth, and distance to the jump). Some relations between the sequent depth ratio, length, and distance of jump and the independent parameters were obtained. Mulahasan et al. [9] investigated the flow parameters around a permeable dike installed in an open channel, the width of which was reduced by one-third. This dyke is filled with two different media possessing distinct properties. When the flow rate values were low, water profile values did not change significantly. However, for higher flowrate values, the variations tend to be more noticeable. Moreover, the effect of the medium's properties was unremarkable.

Some researcher utilized the numerical model in addition to the physical model in their studies. Al-Hashimi et al. [10] developed a 3D numerical model using ANSYS-Fluent to simulate water surface profile over broad crested weir. The model was verified using an experimental data. The result showed good agreement between the two models in terms of determining the discharge coefficient. Yildiz et al. [11] predicted the position of hydraulic jump that occurs for flow passing under a sluice gate. The researchers used experimental models and the computational fluid dynamics (CFD) model to simulate different flow conditions for different gate openings. The outcome of CFD was comparable to the investigational outcomes. Muhsun et al. [12] derived a new formula using ANSYS-Fluent to estimate the flowrate values passing over a broad crested weir with a sharp edge. The authors rely on the correlation between the critical depth and the water depth at the section at the terminal edge of the weir. The level of confidence in the generated formula was examined using a number of standard error indices. The analyses showed high accuracy close for expending the method in predicting the flow rate values over a broad weir. Al-Hashimi et al. [13] conducted a 3D numerical model using CFD technique to simulate flow patterns over a bridge obstruction. The predicted free water surface profile and the longitudinal velocity flow were verified using experimental results. The results showed that the predicted water surface profiles were comparable with the measured data for the two flow categories tested, namely, overtopping flow and full orifice flow.

Hafnaoui et al. [14] used MATLAB® as a programming tool to implement the McCormack finite difference method and 1D Saint–Venant equations the with TVD extension scheme. This simulation aimed to replicate a hydraulic jump formed in sloped channels with a prismatic shape. The authors used different rectangular and triangular sections. The experimental model was applied to analyze the accuracy of the numerical model in predicting the location of the hydraulic jump in different sections. The results obtained by the experimental and numerical models are consistent, especially for conditions of low slopes. These findings suggest that the prediction of jump location was highly affected by the change in the channel slope and Froude number.

Although previous investigations have explored the characteristic of hydraulic jumps, information on the effect of tail water depth or sequent depth on these characteristics, especially its location, was limited. In addition, the majority of researchers have presented their findings through physical models. Nevertheless, some researches have conducted computational software to discover hydraulic jump properties. For example, Hafnaoui et al. [14] used MATLAB® as a programming tool, and Yildiz et al. [11] applied the CFD technique only for a qualitative comparison. Therefore, the hydraulic jump characteristics were further examined in terms of position, length, and velocity distribution. The objective was accomplished using the ANSYS-Fluent model with a fully 2D turbulent model and volume of fluid (VOF) methodology, facilitated by the CFD technique. In addition, this study exhibits the important insights into the hydraulic jump properties provided by the numerical Fluent model as well as the magnitude of the mismatch between experimental results and numerical outputs. The local scour induced by the formation of hydraulic jumps downstream of weirs could compromise the overall stability of the structure or, in extreme cases, lead to its complete collapse. Therefore, accurate prediction of the position of the hydraulic jump for different downstream flow conditions is relatively important. However, the key inquiry pertains to whether the Fluent can reproduce the actual flow characteristics for different flow conditions.

The following sections present the description of the experimental tests in the laboratory, as well as the governing equations and numerical scheme used to simulate the hydraulic jumps. Then, the results of the numerical simulations in rectangular channels for different tail water depths are presented and discussed to predict accurately the hydraulic jump location for all hydraulic jump tests.

2. THEORETICAL BACKGROUNDS

The hydraulic jump occurs when water enters turbulence while the flow regime changed from subcritical to supercritical. Hydraulic jump poses a great danger when it occurs uncontrolled in open channels because of the great forces that arise and the increase in flow depth after the jump. A control hydraulic jump, on the contrary, provides benefits.

Flow enters the channel at depth (y_1), and depths after a hydraulic jump become (y_2). Based on pressure momentum, the expression for the hydraulic jump could be written as follows [15]:

$$\frac{y_2}{y_1} = \frac{1}{2}\left[\sqrt{1 + 8F_{r_1}^{\ 2}} - 1\right] \tag{1}$$

The energy loss on the jump within horizontal channel is given by:

$$\Delta E = \frac{(y_2 - y_1)^3}{4y_1 y_2} \tag{2}$$

$$\eta = \frac{E_2}{E_1} = 1 - \frac{\Delta E}{E_1} \tag{3}$$

where, y_1 indicates the flow depths before the hydraulic jump, y_2 represents the flow depths after the hydraulic jump, Fr_1 is the Froude number in supercritical flow, and ΔE is the dissipated energy in the hydraulic jump. E_1 is the initial specific energy, E_2 is the sequent specific energy, and η is the ratio of dissipate energy through jump.

The sketch for the model used with the fundamental variables is shown in Figure 1. The relevant parameters are as follows:

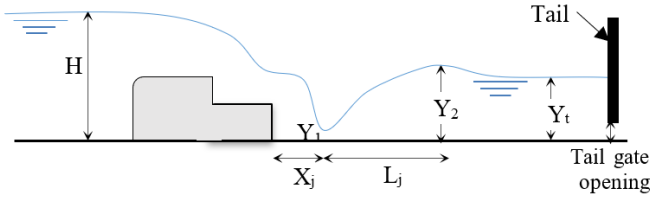

Figure 1. Descriptive illustration of geometrical with hydraulic parameters

$$f\ (V_1, L_i, X_j, H, Y_1, Y_2, Y_t, E_1, E_2, \mu, \rho, g) = 0 \tag{4}$$

where, V_1 is the mean velocity at lowest water depth (Y_1), ρ is the water density, μ is the water viscosity, Y_1 is water depth at the vena contracta, Y_2 is the backup water depth (sequent depth), Y_t is the tailwater depth, E_1 is the initial specific energy, E_2 is the sequent specific energy, g is the gravitational acceleration, L_j is the hydraulic jump distance between the conjugate depths, and X_j is the position of the jump from the downstream toe of the weir.

$$E_1 = y_1 + \frac{V_1^2}{2g} \tag{5}$$

$$E_2 = y_2 + \frac{V_2^2}{2g} \tag{6}$$

Applying the Π-theorem with the independent variables (ρ, V, and Y_1), the following dimensionless groups can be driven:

$$\frac{\triangle E}{E_1} = \left(\frac{X_j}{L_j}, \frac{H}{y_1}, \frac{y_t}{y_1}, F_r, R_1\right) \tag{7}$$

where, $\triangle E = E_1 - E_2$ and (F_r, R_1) represent the Froude number and Reynolds number at vena contracta, respectively.

$$F_r = \frac{V}{\sqrt{gy}} \tag{8}$$

The influence of tail water height on the characteristics of hydraulic jump formed downstream of the stepped weir is presented in this study. The hydraulic jump is created to dissipate the energy of flow coming after the weir. However, the position of the hydraulic jump in the channel should be known exactly to prevent damage to surrounding structures.

3. EXPERIMENTAL SETUP

The experimental investigations were conducted in the hydraulic laboratory at the college of engineering at Musatnsiriyah University, Iraq. A flume of 4.6 m long, 0.3 m wide, and 0.3 m deep was used. The flume is made of acrylic with steel frames for visual investigation of the flow characteristics. The flow at the downstream was controlled by a tailgate located at the end of the flume. The one-stepped weir apron is made of wood coated with a water proof material and installed at a distance of 0.9 m from the inlet. The weir dimensions are as follows: height of 0.15 m, crest width of 0.24 m with an upstream rounded edge, and one step of 0.16 m wide and 0.075 m high. Water was supplied from the pump located in the storage tank through a supply pipe. The flow of the pumped water from the storage tank into the rectangular flume was regulated by an inlet valve. Along the top edges of the flume, three movable point gauges with a precision of 1 mm were installed along the centerline for water level measurements. In addition, a traverse apparatus was positioned at different static points along the flume. Figure 2 shows the detailed variables of the tested model.

Sixteen experimental tests were conducted using four different values of flow rates at 10, 15, 20, and 25 m^3/hr, depending on the power of pump at the supply tank U/s flume. The downstream tailgate opening was adjusted within the range of (0.5-3.3) cm to obtain the required conditions with different tail water depths, Y_t, depending on the dimension of flume that allows the hydraulic jump to develop throughout the flume downstream the weir.

Figure 2. Layout of the flume and experimental setup

4. NUMERICAL MODEL

The ANSYS-Fluent code is a numerical tool that uses the finite volume method to transform governing equations into algebraic equations for numerical solutions. The Naiver–Stokes (NS) equations are used, with time average velocity, resulting in Reynolds averaged NS (RANS) equations. These equations are nonlinear, posing remarkable challenges when solving them analytically, especially for turbulent flow. The governing equations of numerical modeling in ANSYS-Fluent software for unsteady incompressible 2D multi-phase (air and water) flows over weirs are applied to simulate the flow over weir. The continuity and NS equations are described by the differential equations, as follows [16]:

Continuity equation,

$$\frac{\partial}{\partial x_j}(u_j) = 0 \tag{9}$$

Momentum equation,

$$\frac{\partial u_i}{\partial t} + (u_j)\frac{\partial u_i}{\partial x_j} = -\frac{\partial}{\partial x_i}\left(\frac{P}{\rho}\right) + (v_t + v)\frac{\partial}{\partial x_j}\left[\frac{\partial u_j}{\partial x_i} + \frac{\partial u_i}{\partial x_j}\right] - \frac{2}{3}\frac{\partial k}{\partial x_j} + F_i \tag{10}$$

The commonly used and validated multiphase solver VOF is applied to simulate the interaction of air and water multi-phase flow. The realizable (k − ε) turbulent model can be used in this study. The term realizable indicates that the model satisfies certain mathematical constraints on the normal stresses, consistent with the physics of turbulent flows. For example, the Boussinesq relationship and the eddy viscosity definition are combined to obtain the following expression for the normal Reynolds stress in an incompressible strained mean flow [17].

Transport equation of *F* is,

$$\frac{\partial F}{\partial t} + \frac{\partial (F u_j)}{\partial x_j} = o \tag{11}$$

k- equation,

$$\frac{\partial k}{\partial t} + u_j \left(\frac{\partial k}{\partial x}\right) = \frac{\partial}{\partial x_j}\left[v_k \frac{\partial k}{\partial x_j}\right] + v_t \frac{\partial u_i}{\partial x_j}\left[\frac{\partial u_j}{\partial x_i} + \frac{\partial u_i}{\partial x_j}\right] - \varepsilon \tag{12}$$

ε- equation,

$$\frac{\partial \varepsilon}{\partial t} + u_j \frac{\partial \varepsilon}{\partial x} = \frac{\partial}{\partial x_j}\left[v_\varepsilon \frac{\partial \varepsilon}{\partial x_j}\right] + C_a \frac{\varepsilon}{\kappa} v_t \frac{\partial u_i}{\partial x_j}\left[\frac{\partial u_j}{\partial x_i} + \frac{\partial u_i}{\partial x_j}\right] - C_b \frac{\varepsilon^2}{\kappa} \tag{13}$$

$$v_k = \frac{v_t}{\sigma_k} + v \tag{14}$$

$$v_t = C_u \left(\frac{\kappa^2}{\varepsilon}\right) \tag{15}$$

$$v_\varepsilon = \frac{v_t}{\sigma_\varepsilon} + v \tag{16}$$

where, x_j indicates Cartesian coordinate u_i; j is velocity, ρ is fluid density, F_i indicates gravity force components, p represents the pressure of fluid, k is the turbulent kinetic energy, v_t is the eddy viscosity, ε is the rate of dissipation of the kinetic energy, and v is fluid kinematic viscosity. The k-ε model constant values are obtained as follows:

C_u= 0.09, σ_k=1.00, σ_ε=1.30, C_a= 1.44, and C_b= 1.92.

The geometry of the weir performed in the current study was designed using the package plan models. To achieve an accurate simulation, the grid was selected to fit the details of the geometry with a reasonable size to reduce time consumed. Grid size is important in the numerical simulation because it affects not only the accuracy of the result, but also the simulation time. The optimal grid was selected after thorough iterations, using Multizone Quad/Tri method with a grid size of 8 mm. In addition, surface refinement with a grid size of 3.5 mm was used to enhance the representation of the weir faces and the downstream edge of the flume ad to make sure that the tail gate openings were easily recognized. This refinement ensures the easy identification of the tailgate openings. The final grid was generated after several iterations, the optimum mesh of 21435 nodes and 20787 elements was selected to simulate the case study, as shown in Figure 3. The quality of the elements is also considered with appropriate conditions in all simulated models (0.4 < Orthogonal Quality < 1.0); skewness was measured below 0.9. The jump position can be predicted satisfactorily for ordinary engineering applications when a suitable grid size is set.

The boundary conditions were defined as follows:

1. The channel inlet section was categorized into two types; for the lower part, a velocity inlet was implemented with values consistent with experimental works. Meanwhile, for the upper part, a pressure inlet was used with P_{in}=0, and VOF=1 for air.
2. For the outlet section, the boundary condition used for the tail gate openings was pressure outlet P_{out}=0 with, VOF=1 for air. For the upper part, a wall was applied.
3. The channel surface was set as pressure outlet with P_{out}=0 and VOF=1 for air, allowing the model to interpret it as an atmosphere boundary.

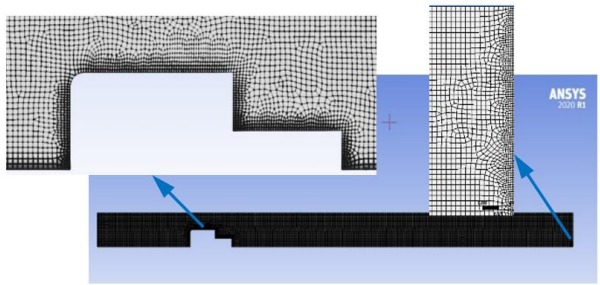

Figure 3. Model meshing setup

In accordance with the implicit scheme for VOF, the following solution methods are selected: the PISO algorithm for the pressure–velocity coupling, PRESTO discretization for pressure, and second-order upwind for momentum. The first-order upwind scheme is selected for turbulent kinetic energy and turbulent dissipation rate. The computational process is executed on a high-performance computer equipped with a Core i7 processor with 16 MB RAM.

5. RESULTS AND DISCUSSION

5.1 Validation of the numerical model

The numerical model implemented using CFD technique model was tested for its capability to study hydraulic jump characteristics. It was validated with a range of hydraulic jumps verified in the flume. The water surface profiles were predicted using VOF method with K-epsilon realizable model. This approach provides satisfactory results regarding free surface flows and recirculation zones and is capable of considering the eddy-viscosity coefficient Cu as a function of local flow characteristics. As a result, the locations of the water surface obtained by numerical solutions are more reliable than the observed data, as shown in Figure 4.

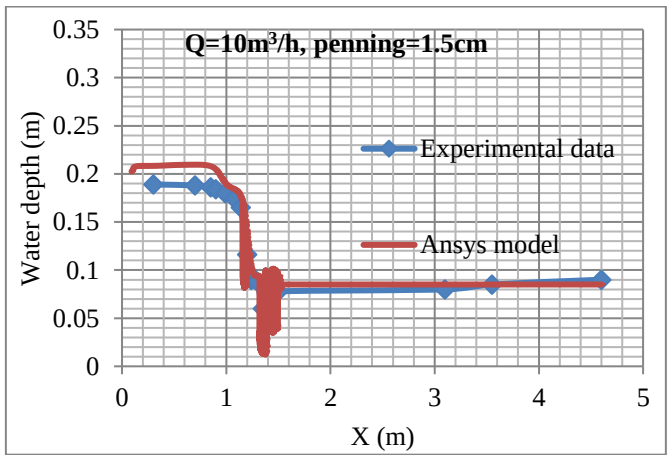

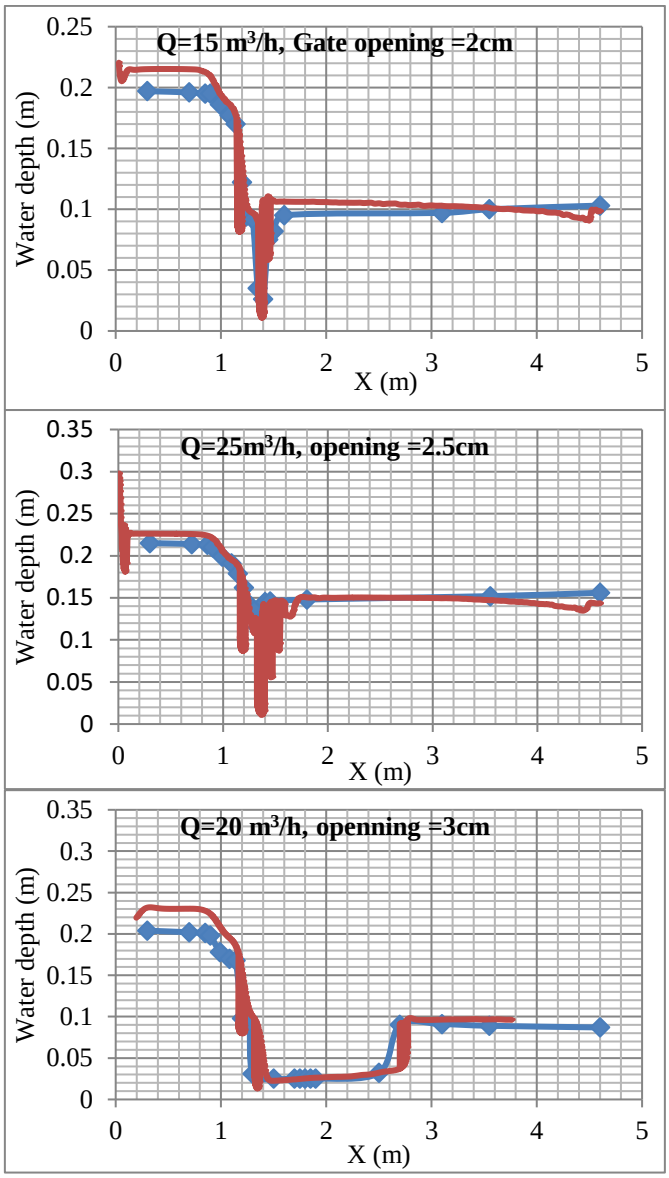

Figure 4. Comparison of the simulated and the laboratory water surface profiles with different flow rate values and different tail gate opening

To determine the degree of error and accuracy between the findings of the experiments and the simulation, Table 1 presents a statistical analysis utilizing some of the standard error indexes reflected in Eqs. (17) to (20) for various samples obtained from laboratory experiments. The statistical analysis' findings indicate that the actual results and those from the CFD simulated model are consistent. This finding suggests that the simulation models developed by ANSYS software can reliably examine the hydraulic jump's characteristics and provide the required solution with a sufficient level of accuracy without the need for actual experiments, thereby saving time, money, and effort [18].

$$RMSE = \sqrt{\frac{1}{n}\sum_{i=1}^{N}(c_m - c_s)^2} \quad (17)$$

$$MSE = \frac{1}{n}\sum_{i=1}^{N}(c_m - c_s)^2 \quad (18)$$

$$MAE = \frac{1}{n}\sum_{i=1}^{N}|c_m - c_s| \quad (19)$$

$$RSE = \frac{\sum_{i=1}^{N}(c_m - c_s)^2}{\sum_{i=1}^{N}(c_m - \overline{c_m})^2} \quad (20)$$

RMSE represents the root mean squared error, whereas MSE, MAE, and RSE represent the mean squared error, the mean absolute error, and the relative square error, respectively. c_m is the actual value, and c_s is the matching simulated value; the mean of the actual values is represented by ($\overline{c_m}$).

Table 1. Test for statistical analysis verification using a few common index errors

Test	RMSE	MSE	MAE	RSE
Q=10, Y_2=0.08, X_j=1.82	0.2357	0.0563	0.1789	0.2325
Q=10, Y_2=0.09, X_j=1.5	0.2439	0.0502	0.1756	0.2129
Q=10, Y_2=0.095, X_j=0.88	0.0341	0.002	0.0435	0.0154
Q=15, Y_2=0.095, X_j=1.6	0.0234	0.0006	0.0243	0.0235
Q=15, Y_2=0.082, X_j=2.35	0.1766	0.0372	0.0854	0.4585
Q=15, Y_2=0.075, X_j=2.65	0.1903	0.0181	0.1122	0.2274
Q=20, Y_2=0.099, X_j=1.8	0.1834	0.0161	0.0968	0.2274
Q=20, Y_2=0.12, X_j=0.6	0.0521	0.0540	0.0677	0.2394
Q=30, Y_2=0.1, X_j=2	0.1643	0.0242	0.0889	0.1325
Q=30, Y_2=0.12, X_j=1.4	0.0453	0.0784	0.2498	0.2345

5.2 Hydraulic jump position

Tail depth influences the hydraulic jump's properties. The jump propagates upstream when the flow over the weir encounters a tail depth greater than the sequent depth, and it moves downstream when the tail depth is less than the sequent depth. The characteristics of the jump depend on where it is located. The closer the jump is to the weir, the clearer it is (in terms of its mixing with the air) and the greater its length and height.

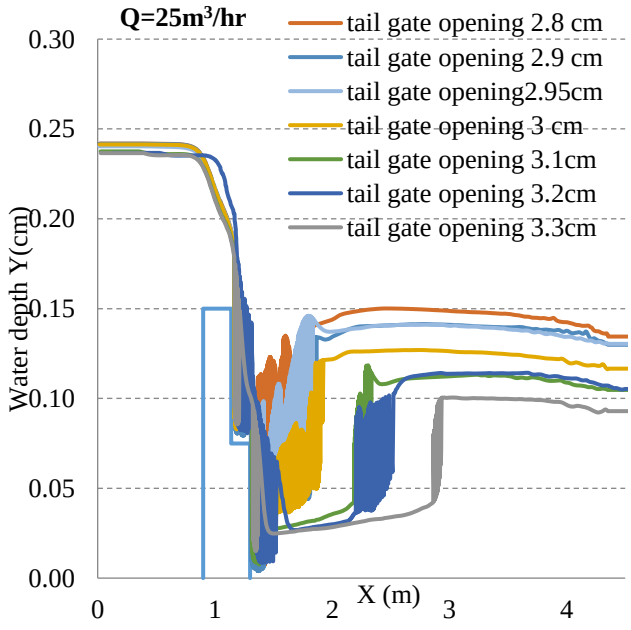

Figure 5. Hydraulic jump profiles predicted by numerical simulations with flowrate value=25 m³/hr for different tail gate opening

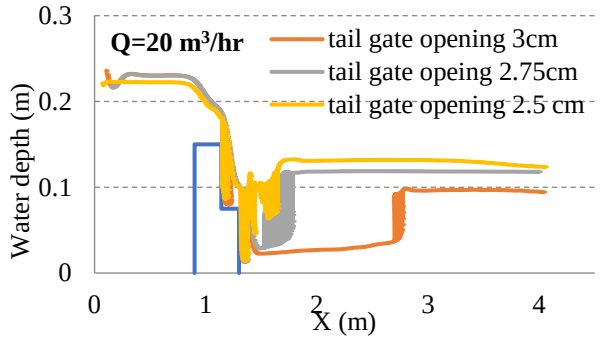

Figure 6. Hydraulic jump profiles predicted by numerical simulations with flowrate value=20 m^3/hr for different tail gate opening

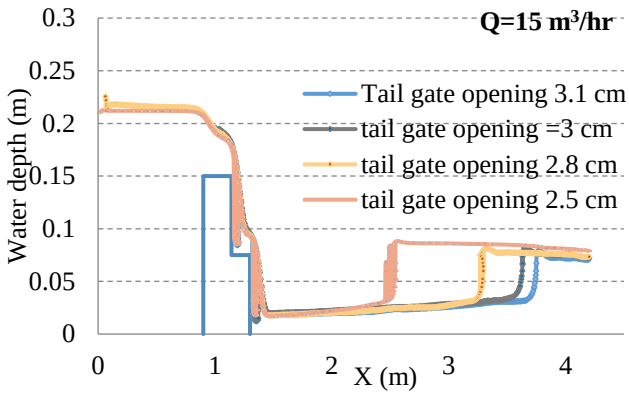

Figure 7. Hydraulic jump profiles predicted by numerical simulations with flowrate value=15 m^3/hr for different tail gate opening

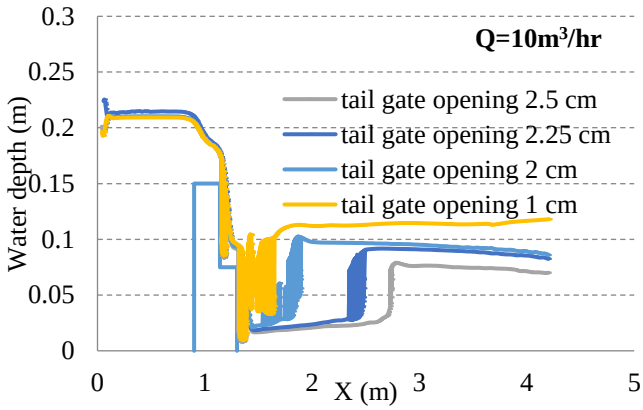

Figure 8. Hydraulic jump profiles predicted by numerical simulations with flowrate value=10 m^3/hr for different tail gate opening

The computational simulation in the rectangular horizontal channel is provided in this section. The numerical model's initial conditions were the same as those used in the tests. The analyses are conducted for a number of scenarios with different discharge values: 25, 20, 15, and 10 m^3/hr and different tail gate openings. Figures 5 to 8 present water surface profiles for each flowrate values. The distance to hydraulic jump (X_j) increases as the sequent depth decreases due to increasing tail gate opening. The results of the free jump were obtained, and all scenarios with the results of the submerged jump were excluded because the locations of such jump cannot be measured.

The results shown in Figures 5 to 8 were analyzed. For instance, at 2.5 cm opening of the tail gate and high Froude numbers, the hydraulic jump is located at channel upstream. However, for the same opening and with low value of Froude numbers, the hydraulic jump is located at the downstream channel. As the tail gate opening increases, the jump propagates more toward the downstream. For most flow conditions, the depth of the tail water is slightly lower than the second depth of the hydraulic jump (sequent depth) especially for the cases of large tail gate opening that is used for higher flowrate values. This value is larger than the sequent depth for some cases (Q=10 m^3/hr, opening= 1 cm) because of the back water curve formed.

5.3 Roller length

To simulate the two phases, air and water, considered in this study, the VOF method with implicit discretization was used. Each phase is represented by its volume fractions and independently satisfies the principles of conservation of mass and momentum. The volume of fraction presented in Figures 9 to 12 show the roller lengths and jump lengths for all flow conditions. The air phase is presented in blue, and the water phase is presented in red. The roller length is represented by the colors between red and blue, indicating the air entry region as shown in the mentioned figures.

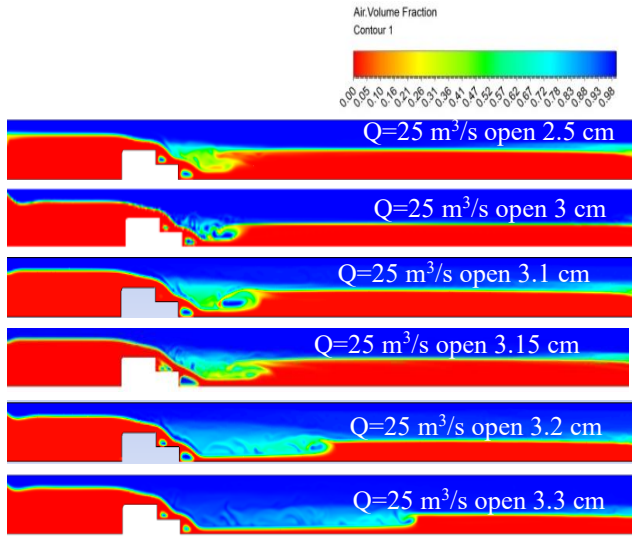

Figure 9. Numerical contour of water surface profile for predicting hydraulic jump locations with flowrate value=25 m^3/hr for different tail gate opening

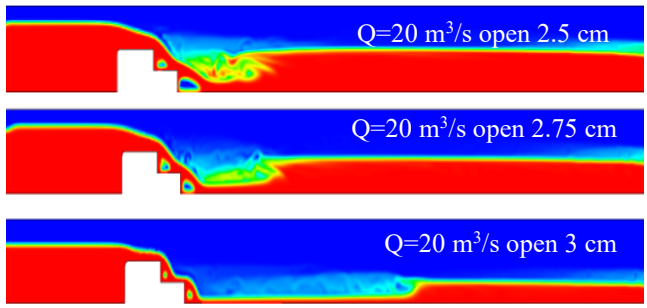

Figure 10. Numerical contour of water surface profile for predicting hydraulic jump locations with flowrate value=20 m^3/hr for different tail gate opening

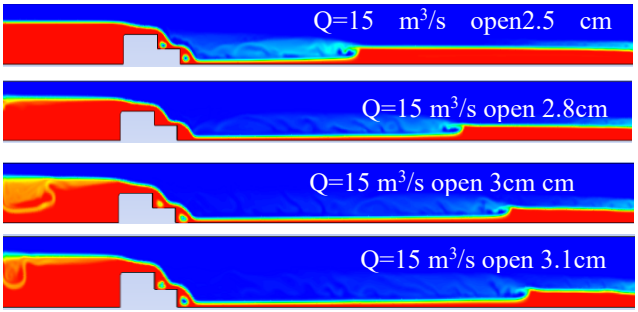

Figure 11. Numerical contour of water surface profile for predicting hydraulic jump locations with flowrate value=15 m^3/hr for different tail gate opening

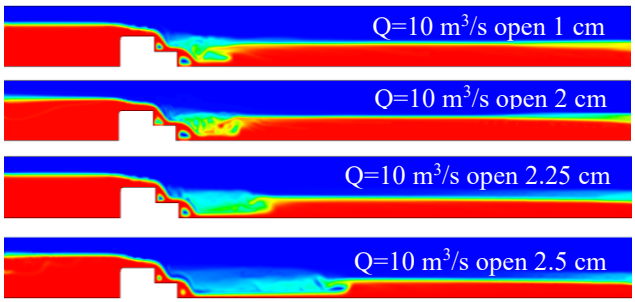

Figure 12. Numerical contour of water surface profile for predicting hydraulic jump locations with flowrate value=10 m^3/hr for different tail gate opening

Rajaratnam [19] defined the length of the jump as the distance, where the mean elevation is at its maximum and the free-surface becomes horizontal. This finding suggests that the jump length is consistently larger than the roller length, which is the distance of the air entry into the water [20].

The figures show that when the jump is located at the upstream, the roller is more noticeable than the jump at the downstream. This finding is due to the fact that the hydraulic jumps with larger downstream conjugate depth have shorter roller lengths and high rate of air entry. On the contrary, the jump with less downstream conjugate depth has longer roller length with less air entry rate, as shown in Figure 13.

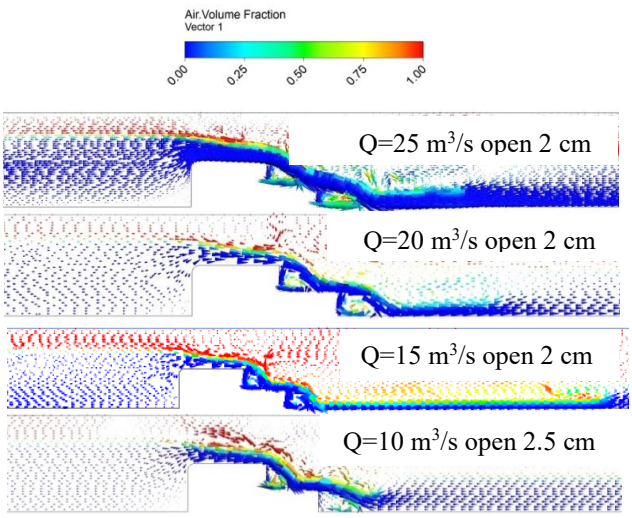

Figure 13. Volume of fraction of water surface profile for different flowrate and different tail gate opening viewing the velocity vectors

5.4 Velocity contour

Figures 14 and 15 present the velocity contours for some downstream flow conditions. The highest velocity is found over the stepped weir and at its end, and the hydraulic jump formed in the vicinity of the hydraulic structure is considered an energy dissipator. The flow velocity value begins to decrease and continues to decrease until it reaches a stable rate at the end of the hydraulic jump and until the flow meets the tail water depth. The nappe falls completely on the weir, as shown by the low flow rate values (10 and 15 m^3/h). This flow regime is known as the nappe flow in terms of stepped weirs, which can be described as a series of free-falling water jets cascading from one step to the next. When the jump is located near the weir, the high velocity values are restricted with a smaller length than the jump located far from the weir due to the further increase in tail gate opening. As a result, the jump propagates toward the channel's downstream. A high velocity is found for a longer length until the jump is formed to dissipate the flow energy. This case might be undesirable because it may cause erosion of the channel's bed. However, the jump becomes undular with lower relative height and exhibits longer roller lengths with less air entry than the jump located near the weir.

Figure 16 presents the relation between the tail depth ratio and Froude number (F_{r1}). As the Froude number increases, the ratio of tail water depth for the same opening also increases. This finding has been proven by previous researchers, such as Ranga Raju [15] and Rajaratnam [19].

Figure 16 further shows a comparison between the sequent depth ratio (Y_2/Y_1) using equations of Ranga Raju [15] and Rajaratnam [19] with the observed data and numerical data for the current study on different inlet conditions. The figure demonstrates that most of the numerical data are between the experimental and previous models. Thus, the present model shows good accuracy.

Figure 17 also depicts the relationship between the hydraulic jump's length ratio and the tail depth ratio for various initial Froude number values with different tail gate openings. The figure shows that the length of the jump increases as the tail water increases for all values of Froude number. When the jump is located at the upstream of the channel, it becomes stronger with height with a more noticeable roller than the jump formed at the downstream of the channel.

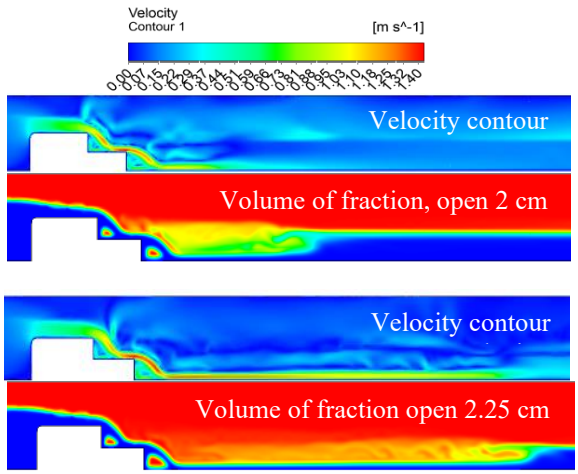

Figure 14. Velocity contour for flowrate=10 m^3/hr, with opening=2 cm and 2.25 cm

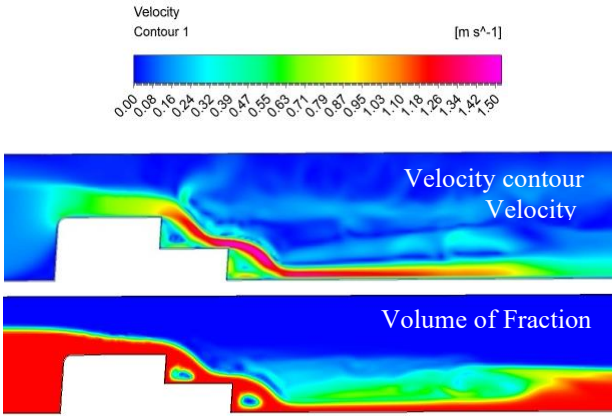

Figure 15. Velocity contour for flowrate=15 m^3/hr, opening=2.5 cm

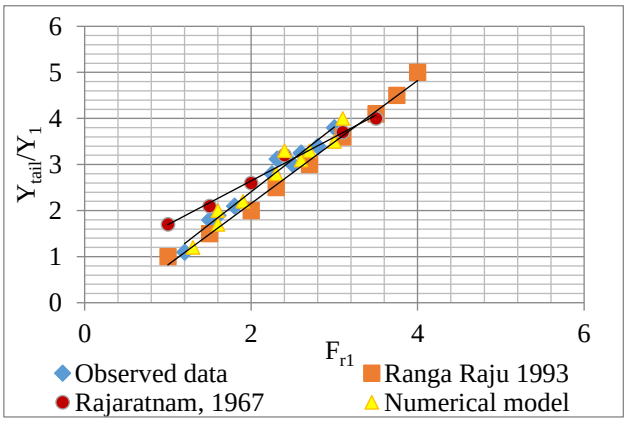

Figure 16. The relation between the tail depth ratio and Froude number

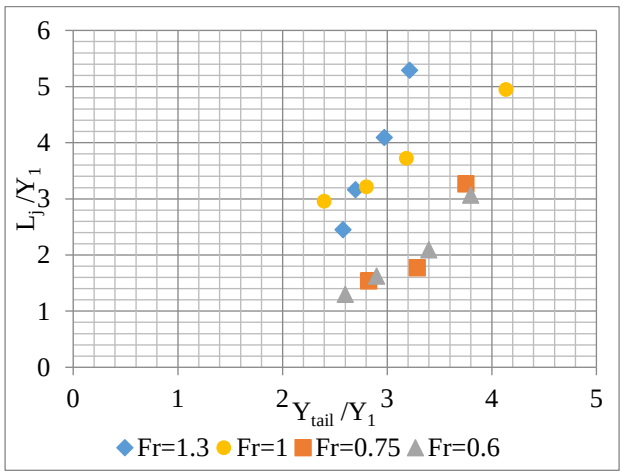

Figure 17. The hydraulic jump length and the tail depth ratios relationships for different values of initial Froude number

Figure 18 presents the variation of relative distance to hydraulic jump length with conjugate depth ratio for different values of Froude number. When the jump is located at the upstream sequent depth Y2 increases. On the contrary, when the jump propagates toward the downstream, the Y2 decreases. This finding is attributed to the fact that when Ytail is larger than Y2, the jump is found at the upstream near the weir. However, the hydraulic jump moves toward the downstream of the channel when Ytail is less than Y2. Figure 18 further shows that the distance to hydraulic jump X_j increases as the depth ratio decreases. Moreover, for the same value of Y_t, the distance to hydraulic jump increases as Froude number decreases.

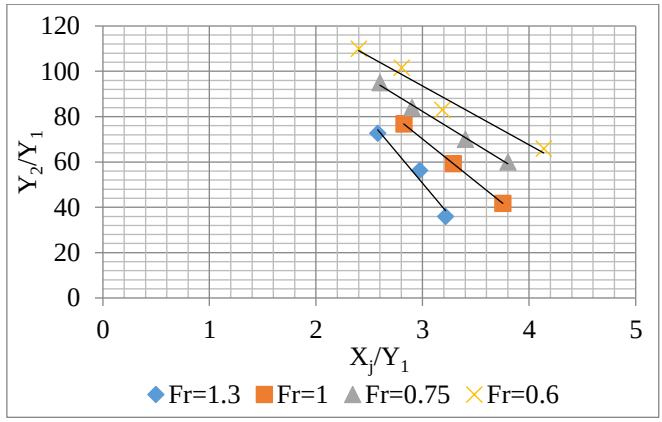

Figure 18. Variation of relative distance to hydraulic jump length with sequent depths ratio for different values of approach Froude number

6. CONCLUSIONS

The numerical model using Fluent–ANSYS successfully exhibits the behavior of the hydraulic jump that is conducted in the experiment. The water surface profile of the numerical model was compared with that of the physical model, and the comparison shows good agreement. Thus, the numerical model successfully determined the position and other characteristics of the jump. The higher Froude numbers indicates that the hydraulic jump is closer to the weir, maintaining constant tail gate opening. Meanwhile, for the same opening but with lower value of Froude number, the hydraulic jump is found at channel downstream. This finding agrees with the experimental models and with the previous studies as well. Therefore, the characteristics of the hydraulic jump can be assessed, and the appropriate solution with a sufficient level of accuracy can be obtained without the requirement for actual experiments and only using simulation models made by ANSYS software. This finding indicates that any uncertainties can be avoided given the high-velocity measurements of the experimental model.

The success of the numerical model can be improved by simulating a large-scale channel with a wide range of flow initial conditions. In the present study, high values of Froude number cannot be simulated due to model scale restrictions in physical and numerical models with the same scale. Therefore, we recommend considering a large scale for numerical model not only to achieve higher Froude numbers but also more reliable results to avoid any uncertainty caused by small velocity values in the numerical simulations. On the contrary, relationships between study variables with wide ranges are derived. However, the question is whether the use of a large scale for numerical model affects the results, especially, with high Froude number, which causes difficulties in predicting the location of the jump.

ACKNOWLEDGMENT

The authors would like to express their gratitude for the

support given by Mustansiriyah University (www.uomustansiriyah.edu.iq) Baghdad, Iraq. The authors are grateful to the Hydraulic Laboratory staff in the College of Engineering for their support and assistance with the experiments.

REFERENCES

[1] Salmasi, F., Özger, M. (2014). Neuro-fuzzy approach for estimating energy dissipation in skimming flow over stepped spillways. Arabian Journal for Science and Engineering, 39: 6099-6108. https://doi.org/10.1007/s13369-014-1240-2

[2] Al-Husseini, T.R., Hamad, H.T., Al-Madhhachi, A.S.T. (2021). Effects of an upstream sluice gate and holes in pooled step cascade weirs on energy dissipation. International Journal of Civil Engineering, 19: 103-114. https://doi.org/10.1007/s40999-020-00568-7

[3] Khatibi, R., Salmasi, F., Ghorbani, M.A. (2014). Modelling energy dissipation over stepped-gabion weirs by artificial intelligence. Water Resources Management, 28: 1807-1821. https://doi.org/10.1007/s11269-014-0545-y

[4] Sauida, M.F., Ahsan, A. (2022). Simulation of relative energy loss downstream of multi-gate regulators using ANN. Cogent Engineering, 9(1): 2017388. https://doi.org/10.1080/23311916.2021.2017388

[5] Ibrahim, M.M., Refaie, M.A., Ibraheem, A.M. (2022). Flow characteristics downstream stepped back weir with bed water jets. Ain Shams Engineering Journal, 13(2): 101558. https://doi.org/10.1016/j.asej.2021.08.003

[6] Felder, S., Montano, L., Cui, H.W., Peirson, W., Kramer, M. (2021). Effect of inflow conditions on the free-surface properties of hydraulic jumps. Journal of Hydraulic Research, 59(6): 1004-1017. https://doi.org/10.1080/00221686.2020.1866692

[7] Mohammadi, M., Nazari-Sharabian, M., Karakouzian, M. (2021). A novel analytical method for evaluating the characteristics of hydraulic jump at a positive step. Water (Switzerland), 13(15): 2005. https://doi.org/10.3390/w13152005

[8] Abdel-Mageed, N. (2015). Effect of channel slope on hydraulic jump characteristics. Physical Science International Journal, 7(4): 223-233. https://doi.org/10.9734/psij/2015/18527

[9] Mulahasan, S., Saleh, M.S., Muhsun, S.S. (2021). Simulation of flow around a permeable dike using physical and 3D-CFD models. International Journal of River Basin Management, 21(1): 53-65. https://doi.org/10.1080/15715124.2021.1901726

[10] Al-Hashimi, S.A.M., Saeed, K.A., Nahi, T.N. (2019). Experimental and CFD modeling of hydraulic jumps forming at submerged weir. Journal of the Institution of Engineers (India): Series A, 100: 487-493. https://doi.org/10.1007/s40030-019-00381-z

[11] Yildiz, A., Marti, A.I., Yarar, A., Yilmaz, V. (2020). Determination of position of hydraulic jump in a flume by using CFD and comparison with experiential results. Romanian Journal of Ecology & Environmental Chemistry, 2(2): 78-85. https://doi.org/10.21698/rjeec.2020.211

[12] Muhsun, S.S., Al-Hashimi, S.A.M., Al-Osmy, S.A.T. (2020). CFD simulation model and experimental study to implement a new flowrate formula for a rounded broad crested weir considering the end depth as control section. Periodicals of Engineering and Natural Sciences, 8(2): 809-820. http://doi.org/10.21533/pen.v8i2.1295

[13] Al-Hashimi, S.A., Al-Osmy, S.A., Mulahasan, S.A.A.D. (2020). Water surface profile and flow pattern simulation over bridge deck slab. Journal of Engineering Science and Technology, 15(1): 291-304.

[14] Hafnaoui, M.A., Carvalho, R.F., Debabeche, M. (2016). Prediction of hydraulic jump location in some types of prismatic channels using numerical modelling. In 6th IAHR IJREWHS, Lübeck, Germany. https://doi.org/10.15142/T3D01F

[15] Ranga Raju, K.G. (1993). Flow Through Open Channels. Tata McGraw Hills, pp. 196-198.

[16] Versteeg, H.K., Malalasekera, W. (2007). An Introduction to Computational Fluid Dynamics. Pearson Education Limited.

[17] Muhsun, S.S., Al-Madhhachi, A.T., Al-Sharify, Z.T. (2020). Prediction and CFD simulation of the flow over a curved crump weir under different longitudinal slopes. International Journal of Civil Engineering, 18(9): 1067-1076. https://doi.org/10.1007/s40999-020-00527-2

[18] Saleh, M.S., Hamad, H.T. (2020). Forecasting the annual flow rate of the Tigris River using stochastic modelling. Periodicals of Engineering and Natural Sciences, 8(4): 2035-2044. http://doi.org/10.13140/RG.2.2.13933.61929

[19] Rajaratnam, N. (1976). Turbulent Jet. 1st Edition, Elsevier Science.

[20] Al-Husseini, T.R., Al-Madhhachi, A.S.T., Naser, Z.A. (2020). Laboratory experiments and numerical model of local scour around submerged sharp crested weirs. Journal of King Saud University-Engineering Sciences, 32(3): 167-176. https://doi.org/10.1016/j.jksues.2019.01.001

NOMENCLATURE

E_1	initial specific energy, m
E_2	sequent specific energy, m
Fi	gravity force components, $N.m^{-2}$
F_r	Froude number
g	gravitational acceleration, $m.s^{-2}$
H	water depth U/s channel
k	turbulent kinetic energy, kg. m^2. s^{-2}
L_j	hydraulic jump distance between the conjugate depths, m
p	pressure of fluid, $N.m^{-2}$
Q	discharge, $m^3.s^{-1}$
R_1	Reynolds number
V_1	the mean velocity at lowest water depth (Y_1), $m.s^{-1}$
x_j	cartesian coordinate
X_j	position of the jump from the downstream toe of the weir, m
Y_t	tail water depth, m
Y_1	water depth at the vena contracta, m
Y_2	backup water depth, m

Greek symbols

ΔE	energy loss on the jump within horizontal channel, m
ρ	water density

ε rate of dissipation of the kinetic energy, $m^2.\ s^{-3}$
ν fluid kinematic viscosity, $m^2.s^{-1}$
ν_t eddy viscosity, $m^2.s^{-1}$
μ dynamic viscosity, $kg.\ m^{-1}.\ s^{-1}$